Fibers and Polymers 2019, Vol.20, No.8, 1594-1600
DOI 10.1007/s12221-019-9015-8

ISSN 1229-9197 (print version)
ISSN 1875-0052 (electronic version)

Improvement of the Electrospinnability of Silk Fibroin Solution by Atmospheric Pressure Plasma Treatment

Masoud Dadras Chomachayi[1], Atefeh Solouk[2], and Hamid Mirzadeh[1]*

[1]*Polymer Engineering and Color Technology Faculty, Amirkabir University of Technology (Tehran Polytechnic), Tehran 5916-34311, Iran*
[2]*Biomedical Engineering Faculty, Amirkabir University of Technology (Tehran Polytechnic), Tehran 15875-4413, Iran*
(Received January 4, 2019; Revised March 16, 2019; Accepted March 21, 2019)

Abstract: In this study, silk fibroin (SF) was extracted from the silkworm cocoon and fabricated to form a nonwoven mat by electrospinning process. In order to improve the electrospinnability of SF, the polymer solution was treated with atmospheric pressure plasma. Conductivity and viscosity of SF-formic acid solution increased after the plasma treatment. The morphology of SF electrospun scaffolds before and after treatment was investigated by scanning electron microscope (SEM). The results showed that plasma treatment significantly improved the electrospinnability of SF solution and the morphology became fine and bead-less. Furthermore, the results of the fourier-transform infrared spectroscopy (FT-IR) and differential scanning calorimetry (DSC) showed that the plasma treatment increased the crystallinity of SF scaffolds and changed some part of polymer conformation from random coil to β-sheet crystals. Additionally, this method increased the mechanical properties and biodegradation resistance of SF scaffolds.

Keywords: Biomaterials, Porous materials, Silk fibroin, Electrospinning, Atmospheric pressure plasma

Introduction

Tissue engineering aims to assemble functional constructs that can improve or replace injured tissues in the human body [1]. Porous scaffolds play a critical role in tissue engineering due to their unique properties [2]. Electrospinning is an exciting technique to produce the polymeric scaffolds which can imitate the biological function and structure of native extracellular matrix (ECM) of tissues [3]. In this process, under the electric field, electrostatic forces dominate the surface tension of polymer solution and create a charged jet of the solution. The charged jet moves towards the collector and dries with the evaporation of the solvent, therefore leading to the formation of solid micro- and nanofiber of polymers [4]. Various parameters, such as electrical field, solution concentration, flow rate, distance between needle and collector, and humidity of ambient can be manipulated to achieve the favorable structure of nanofiber [5]. The electrospun scaffolds have many desired properties including high porosity, interconnected pores, high surface-to-volume ratio, and controllable *in vivo* mass loss rates [6-8]. Besides these advantages, in some polymeric solutions with low conductivity and high surface tension, the undesired defects like micro-bead appear along the nanofibers. The presences of these defects decrease the mechanical and cellular properties of polymeric scaffolds [2,3]. To address this issue, researchers added additives like salts or even highly polar solvents to the polymeric solution to make suitable solutions for electrospinning [9]. However, this strategy involves safety concerns and additional costs. Moreover, highly polar solvents due to their low vapor tension could not entirely evaporate during the process and toxic traces will be appeared in the produced scaffolds [10]. Therefore, an effective and non-toxic method should be adapted to improve the electrospinnability of some polymeric solutions.

The plasma treatment has been used as one of the environmentally friendly processes for modification of the polymers surface properties [11]. However, common plasma systems need low pressure and vacuum which restricts their application [12]. Recently, atmospheric pressure plasma was known as a new technique to treat the polymeric solution [13]. Shi *et al*. declared that the atmospheric plasma treatment can be used to improve the electrospinnability of the polyethylene oxide (PEO) solution. Results showed that the morphology of nanofibers was significantly improved and defect-free PEO nanofibers were produced after plasma treatment [14].

Silk fibroin (SF) is a fibrous protein which is extracted mainly by silkworm cocoons and spiders. Recently, special attention has been paid to the SF because of its appropriate mechanical properties, nontoxicity, biodegradability, and biocompatibility [15]. Formic acid is a common solvent for fabrication of the SF electrospun scaffolds [16]. However, previous studies showed that the presence of defects and micro-beads on the electrospun nanofibrous of SF-formic acid solutions [17].

In this present study, for the first time, atmospheric pressure plasma treatment has been adopted to improve the electrospinnability of the SF-formic acid solution. The conductivity and viscosity of SF solution were investigated before and after plasma treatment. Moreover, the SF fabricated mats were then characterized by scanning electron microscopy (SEM), differential scanning calorimetry (DSC),

*Corresponding author: Mirzadeh@aut.ac.ir

fourier transform infrared spectroscopy (FT-IR), mechanical test, and *in vitro* mass loss assay.

Experimental

Materials

Bombyx mori silkworm cocoons were obtained from the University of Guilan (Rasht, Iran). Formic acid (98-100 %), sodium carbonate (Na_2CO_3), and lithium bromide (LiBr), and were purchased from Merck (Germany).

Preparation of Silk Fibroin (SF)

Firstly, cocoons of silkworm were boiled for 45 min in an aqueous solution of 0.02 M Na_2CO_3, and then were rinsed for five times with the distilled water. After drying, the degummed SF fibers were dissolved in 9.3 M LiBr at 60 °C for 4 h and dialyzed in a dialysis membrane against distilled water for three days by changing water four times. Finally, the SF solution was poured into a petri dish and dried at room temperature for 24 h [15,18].

Electrospinning of SF Solutions

The polymer solution was prepared by dissolving SF in formic acid at 25 °C and the magnetic stirring was continued for 4 h. The solution was filled into a 10 m*l* plastic syringe and electrospun for 12 h. The parameters of electrospinning including solution concentration, flow rate, distance between needle and collector, as well as voltage were selected at 8-10 w/v%, 0.4 cc/h, 12 cm, and 18 kV, respectively [7,10].

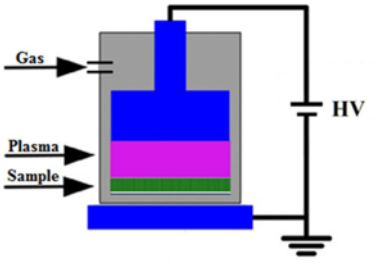

Figure 1. Schematic of atmospheric plasma apparatus.

Atmospheric Pressure Plasma Treatment

The atmospheric pressure plasma apparatus from the Shahid Beheshti University (Tehran, Iran) was used in this study. Figure 1 shows the schematic image of this apparatus. The SF-formic acid solution spilled into a glass beaker and was then placed between the electrode plates of the plasma apparatus as shown in Figure 2. Then, the apparatus was sealed and argon gas was introduced to the chamber. The treatment was carried out for the different plasma voltages (17-25 kV) and treatment times (30-180 sec).

Conductivity and Viscosity

The conductivity and viscosity of SF solution were measured by the Tetracon 325 conductivity meter and the Brookfield viscometer (Model LVDVE 230), respectively.

SEM

The morphological observation of the SF electrospun scaffolds was carried out with the SEM (AIS2100, South Korea). Before the examination, the samples were coated with a thin layer of gold.

DSC

Thermal properties of the SF nanofibrous mat was analyzed by DSC on the Mettler Toledo DSC822E (Schwarzenbach, Switzerland) equipment. The measurements were carried out in the temperature range 140-320 °C and the heating rate of 10 °C/min.

FT-IR

The SF nanofibrous mat was analyzed with FT-IR on the Tensor 27, Brucker Optics (Germany). Samples were scratched into powder, mixed with KBr powder and then compressed into a pellet. The scans were collected under absorbance mode at a spectral range of 400 cm^{-1} to 4000 cm^{-1} at

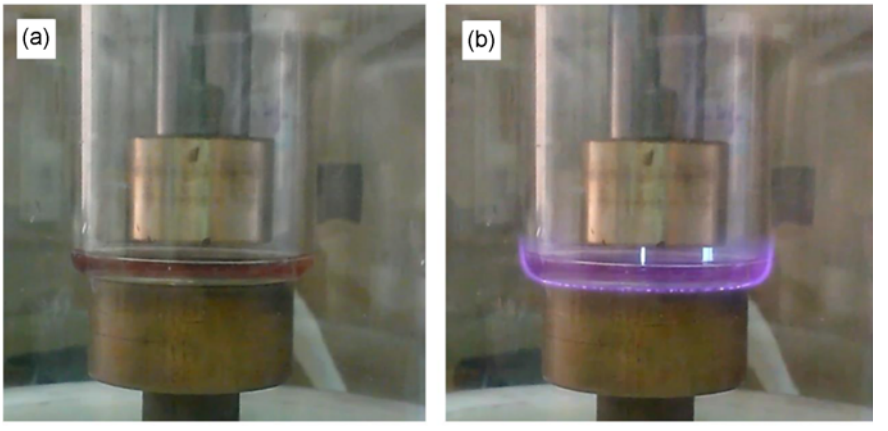

Figure 2. SF solution between two copper electrodes of apparatus; (a) before and (b) under plasma treatment at voltages 25 kV.

a scan resolution of 4 cm^{-1}.

Mechanical Properties

The mechanical property of SF scaffold was measured by a universal testing machine on the Instron 5567 (United States) with 10 N load cell and a cross-head speed of 1 mm/min. The samples were cut into 3×0.5 cm^2. The tensile strength (MPa), Young's modulus (MPa), and elongation at break (%) of the mats were calculated from the obtained stress-strain curves (n=3).

***In Vitro* Mass Loss Assay**

The mass loss of the SF scaffolds was measured in the PBS solution. Firstly, each sample was cut into 1×1 cm^2 and immersed in the PBS solution (pH 7.4) at 37 °C. Then, samples were extracted at different times (1, 2, 3, 7, 14, 21, and 28 day) and the water was removed by filter paper. The mass loss percentage was calculated according to the below equation:

$$\text{Mass loss (\%)} = \frac{W_i - W_f}{W_i} \times 100\% \quad (1)$$

where W_i and W_f are the initial and final mass of the SF scaffolds (g), respectively (n=3).

Results and Discussion

The conductivity of SF-formic acid solution (at 8 w/v% concentration) immediately after treatment is shown in Figure 3(a). It can be observed that the solution conductivity increased after plasma treatment. Atmospheric pressure plasma can ionize the polymer chains and even solvent molecules [6,11]. Consequently, many charged molecules were generated in the polymer solution, which leads to higher conductivity [19,20]. However, as can be seen in Figure 3(b), the conductivity of the SF solution decreased after delay time between the plasma treatment and conductivity measurement. It's may be attributed to the neutralization of charged molecules generated by atmospheric pressure plasma [21]. Moreover, the conductivity values of the plasma-treated solution even after 9 h aging time are greater than the untreated SF solutions (p-value<0.05). Figure 4 illustrated the effect of plasma treatment on the viscosity of the SF solution. As it is shown, the viscosity strongly increased after plasma treatment. It may be due to the strong intermolecular interaction between charged molecules which restricts the mobility of polymer chains [22]. In addition, by measuring the volume of the solution before and after treatment, it was found that the solution concentration somewhat increased from 8 to 8.6 w/v%. It seems that the solvent was evaporated during plasma treatment and leads to higher concentration.

Figure 5(a) and 5(b) show the SEM images of the nanofibrous mats of untreated SF solution at 8 and 10 w/v% concentrations, respectively. As can be seen, there are many

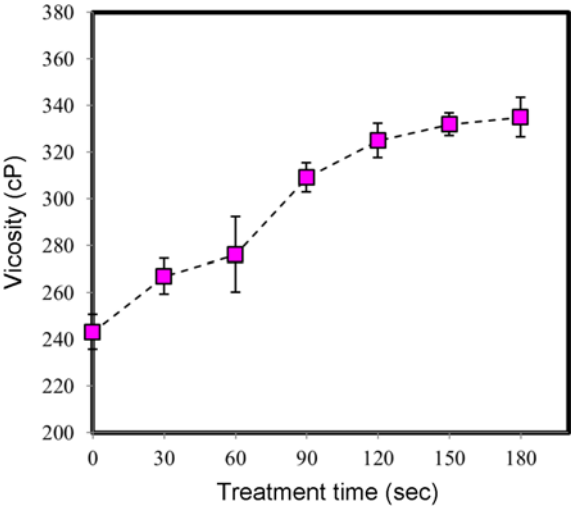

Figure 4. Viscosity of SF solutions at 8 w/v% concentration under different plasma treatment time at voltages 25 kV.

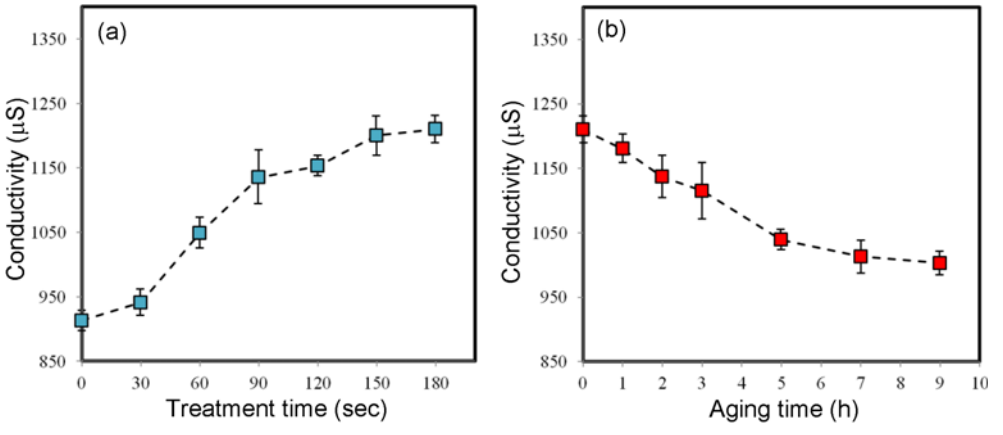

Figure 3. Conductivity of SF solutions at 8 w/v% concentration; (a) under different plasma treatment time at voltages 25 kV and (b) as a function of aging time after plasma treatment.

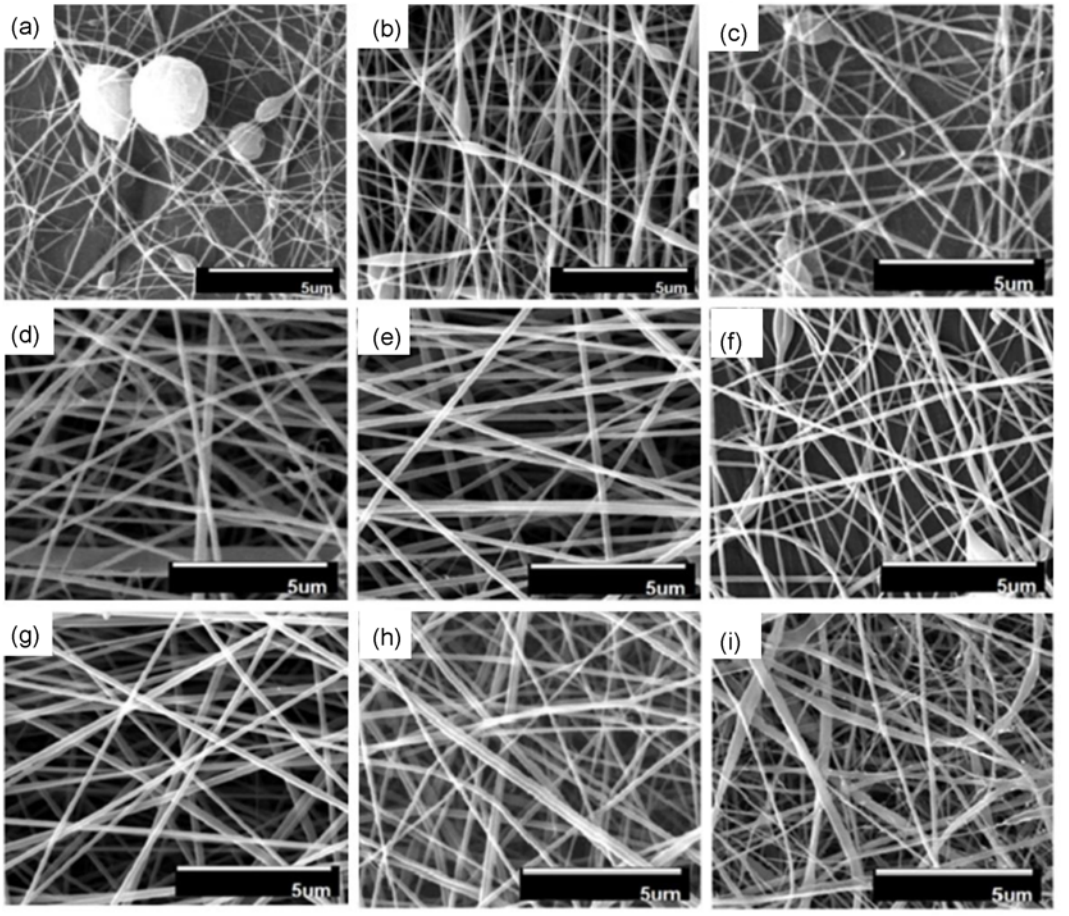

Figure 5. SEM images of SF scaffolds: 1-untreated solution at (a) 8 and (b) 10 w/v% solution concentration. 2-plasma-treated solution (concentration=8 w/v%): effect of plasma voltage=17 kV (c), 21 kV (d), and 25 kV (e) (treatment time=120 sec), effect of treatment time=30 sec (f) and 180 sec (g) (plasma voltage=25 kV), and effect of delay time=2 h (h) and 5 h (i) (plasma voltage=25 kV and treatment time=120 s). Scale bars=5 μm.

defects and micro-beads along the SF nanofibers in Figure 5(a). Experimental findings have shown that the solution concentration is one of the most important parameters in the electrospinning process. Generally, if the concentration is too low, some beads are formed along the fibers. A gradual change in the configuration of beads, from spherical to cylindrical shape occurs with an increase in the concentration. When the concentration is ~2.5 times greater than the entanglement concentration of polymer chains, smooth and bead-free nanofibers are obtained [3]. Accordingly, it can be inferred that for the concentrations about 8 w/v%, the required entanglement between the polymer chains does not exist and a large number of beads are formed along the SF nanofibers. However, while increasing the solution concentration from 8 to 10 w/v%, the morphology became smoother and more bead-free.

The effects of the plasma treatment on the morphology of SF electrospun scaffolds were investigated by SEM observation. As shown in Figure 5(c), the plasma treatment (treatment time=120 sec and voltage=17 kV) did not perfectly prevent the micro-beads formation along the SF nanofibres. Enhancing the voltage to 21 kV resulted in a significant decrease in the presence of micro-beads (Figure 5(d)). Moreover, fine and uniform nanofibers can be seen when the voltage is set at 25 kV (Figure 5(e)). The solution conductivities at 17, 21, and 25 kV voltage were 936±17, 1107±26, and 1153±14 μs, respectively (treatment time= 120 sec). The results implied that the conductivity was increased with increasing the value of voltage. Therefore, in the higher value of solution conductivity, a lower amount of electrostatic force is required to dominate the surface tension of polymer solution [23]. Therefore, more stretching of the polymer charged jet occurs along the electric field and the morphology changes from micro-beads to bead-free nanofibers [24].

Figure 5(e) showed that 120 sec for plasma treatment (voltage=25 kV) is adequate time for achieving the bead-free nanofibers and increasing the treatment time to 180 sec

resulted in no further formation of fine morphology (Figure 5(g)). Furthermore, in order to evaluate the durability of the treatment, the effect of the delay time between the electrospinning process and plasma treatment (aging) was investigated. As can be seen in Figure 5(i), the morphology of SF scaffold became un-uniform and some micro-beads could be observed along the nanofibers. As mentioned previously, the charged molecules were neutralized by increasing the delay time between the plasma treatment and the electrospinning process (Figure 3(b)). Therefore, the effect of plasma treatment to improve the electrospinnability of SF solution decayed after 5 h of delay time.

The FT-IR spectra of SF electrospun scaffolds before and after plasma treatment of solution are given in Figure 6. Intense absorption bands on the FT-IR spectra of SF were observed for amide I, amide II, and amide III at 1655 cm^{-1}, 1538 cm^{-1}, and 1239 cm^{-1}, respectively. Amide I band [1600-1700 cm^{-1}] mainly is related to the ν(C=O) stretching and a small contribution from the δ(N-H) in-plane bending vibration [25]. Amide II band [1510-1560 cm^{-1}] mainly is due to the δ(N-H) deformation and small stretching vibrations of the ν(C-N). Also, amide III band [1200-1300 cm^{-1}] is due to the major contribution originates from the δ(N-H) vibration and small stretching vibrations of the ν(C-N) [13,20]. As can be seen, the intensity of amide peaks increased after plasma treatment of SF solution. Moreover, the small absorption band at 1698 cm^{-1} identified in the amide I peak, which is attributed to the high ordered of β-sheet crystals [21,22,26,27]. SF is a semi-crystalline polypeptide that consists of two structures: amorphous region (random coil) and crystalline antiparallel structures (β-sheet crystal). The β-sheet structure is formed by the hydrogen bonding between N-H and C=O groups of SF chains [28]. The peaks at 1650 cm^{-1} and 1630 cm^{-1} represent the β-sheet and random coil conformation of SF chains, respectively [29]. The percentage of β-sheet crystal in the SF can be calculated with the below equation [30]:

$$\% \beta\text{-sheet} = \frac{A_{1630}}{A_{1650} - A_{1630}} \times 100 \quad (2)$$

where A_{1630} and A_{1650} are the area under the peaks at 1630 cm^{-1} and 1650 cm^{-1}, respectively. The percentages of β-sheets are 58.3 % and 62.1 % for electrospun scaffolds of untreated and plasma-treated SF solution, respectively. It can be explained that charged polymer chains experienced more stretching force and became more aligned compared with the uncharged polymers. Therefore, the probability of the hydrogen interactions between charged chains are increased by plasma treatment and, accordingly, more β-sheet crystals are formed during electrospinning presses.

The non-isothermal DSC thermograms from the second heating cycle of SF electrospun scaffolds and the thermodynamic parameters before and after plasma treatment are given in Figure 7 and Table 1, respectively. As can be seen in the results, the glass transition temperature (T_g), melting temperature (T_m), and melting enthalpy (ΔH_m) were enhanced to higher values after plasma treatment of SF solution (*p*-value<0.05). These changes can be attributed to the increase of the intermolecular interactions between charged chains that cause decreasing of the polymer chains mobility. The exothermic cold crystallization peak was observed in SF scaffolds about 215 °C (T_{cc}) that indicates it has previously been cooled very quickly and had no sufficient time to crystallize. The cold crystallization enthalpy (ΔH_{cc}) of plasma-treated SF was significantly higher than the observed value for the untreated one (*p*-value<0.05). As mentioned previously, plasma treatment increased the solution conductivity and leads to the formation of charged molecules. Therefore, the charged polymer chains were stretched more than uncharged polymers under the electrostatic forces and as a result, the conformation of SF changed from the non-crystalline parts (random coil) to the crystalline structures

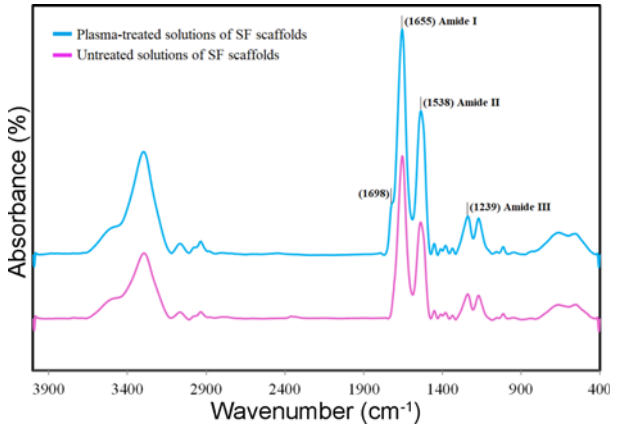

Figure 6. FT-IR of untreated and plasma-treated solutions of SF nanofibrous mats (voltage 25 kV and treatment time 120 sec).

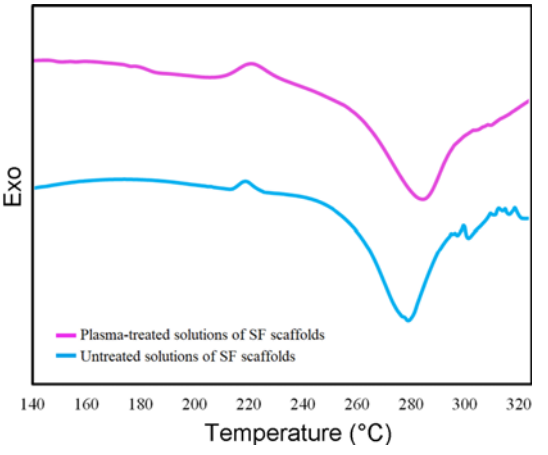

Figure 7. Second heating DSC curves of untreated and plasma-treated solutions of SF nanofibrous mats (voltage 25 kV and treatment time 120 sec).

Table 1. Thermal parameters of SF nanofibrous mats obtained from DSC scans

Sample	T_g (°C)	T_{cc} (°C)	T_m (°C)	ΔH_{cc} (J/g)	ΔH_m (J/g)
SF mat (untreated solution)	181.34±0.76	214.09±0.41	279.11±0.01	8.73±0.32	44.74±0.25
SF mat (plasma-treated solution)	185.67±0.46	215.80±0.70	283.85±1.06	14.17±0.18	56.76±0.16

Figure 8. Schematic of the conformation of SF chains.

(β-sheet) [16,17]. This observation verifies the result of FT-IR. Figure 8 shows a schematic conformation of SF chains after plasma treatment and electrospinning process.

The mechanical property is one of the most important features of scaffolds during the application in tissue engineering. Thus, the uniaxial tensile test was used in order to evaluate the mechanical properties of the SF electrospun scaffolds before and after the plasma treatment of solution. The values of tensile strength (MPa), Young's modulus (MPa), and elongation at break (%) for the scaffolds are detailed in Table 2. According to the results, the scaffold of plasma-treated solution presents higher values of Young's modulus compared with the untreated one (p-value<0.05), while the elongation at break is somewhat lower (p-value< 0.05). It is well known that the degree of orientation and crystallinity of polymer structure determine the mechanical properties of scaffolds [31-33]. Previous studies showed that the crystallinity of SF electrospun is low due to the rapid nanofiber formation during the electrospinning process. Therefore, the modulus of SF nanofibrous scaffold is relatively low [34]. As with the results of FT-IR and DSC, the plasma treatment of the SF solution increased the conformation of polymer chains from random coil to β-sheet crystals, as a result, the modulus of SF nanofibrous was increased. Therefore, the rise in the β-sheet structures would cause an increase in Young's modulus whereas the increase in the random coil region would cause an increase in the final value of elongation at break (the change is not significant for the tensile strength ((p-value>0.05)) [35].

Table 2. Mechanical properties of the untreated and plasma-treated solutions SF nanofibrous mats

Sample	Young's modulus (MPa)	Tensile strength (MPa)	Elongation at break (%)
SF mat (untreated solution)	2.84±0.53	3.05±0.26	9.74±0.12
SF mat (plasma-treated solution)	3.68±0.44	3.72±0.39	8.20±0.61

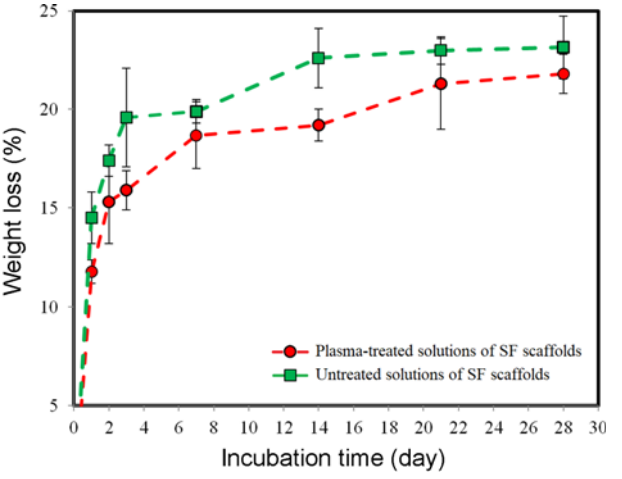

Figure 9. Mass loss percentage of untreated and plasma-treated solutions of SF nanofibrous mats (voltage 25 kV and treatment time 120 sec) in PBS at 37 °C.

Figure 9 illuminates the *in vitro* mass loss of SF electrospun scaffolds before and after the plasma treatment of solution. The scaffolds of untreated and plasma-treated SF solution showed mass reductions of 23.69 % and 21.73 %, respectively, during 28 days immersion in the PBS. SF resists against biodegradation in the aqueous media due to its hydrophobicity and β-sheet crystals, as water molecules cannot penetrate into the crystalline structure [34]. Therefore, it would be expected that the SF scaffolds of the plasma-treated solution should exhibit somewhat lower biodegradation in comparison with untreated one. Moreover, by promoting the mechanical properties, the spaces between the lamellae crystal which favored for the degradation process did not change and the structure resisted to dimensional change when in contact with the PBS [36].

Conclusion

In this study, the SF-formic acid solution was treated with atmospheric pressure plasma. According to the obtained results, it was found that the conductivity and viscosity of the SF solution increased after plasma treatment of solution. The result of the SEM showed that the plasma treatment had a significant effect on the improvement of the electrospinnability of SF solution and the morphology became uniform and bead-free. Also, plasma treatment enhanced the crystallinity of SF structure and the chains conformation can be changed from random coil to β-sheet crystals. Moreover, this approach improved the mechanical properties and biodegradation resistance and it can be concluded that the plasma treatment of SF solution can be proposed for increasing the water stability of scaffolds.

Acknowledgements

This study was financially supported by the Amirkabir University of Technology (Tehran Polytechnic), Grant No. 95.

References

1. A. J. Hassiba, M. E. El Zowalaty, G. K. Nasrallah, T. J. Webster, A. S. Luyt, A. M. Abdullah, and A. A. Elzatahry, *Nanomedicine*, **11**, 715 (2016).
2. H. Chen, R. Truckenmüller, C. Van Blitterswijk, and L. Moroni, "Fabrication of Nanofibrous Scaffolds for Tissue Engineering Applications", pp.158-183, Woodhead Publishing, Netherlands, 2013.
3. K. Garg and G. L. Bowlin, *Biomicrofluidics*, **5**, 13403 (2011).
4. L. Jin, T. Wang, M.-L. Zhu, M. K. Leach, Y. I. Naim, J. M. Corey, Z.-Q. Feng, and Q. Jiang, *J. Biomed. Nanotechnol.,* **8**, 1 (2012).
5. J. Wang, R. Ye, Y. Wei, H. Wang, X. Xu, F. Zhang, J. Qu, B. Zuo, and H. Zhang, *J. Biomed. Mater. Res. Part A*, **100**, 632 (2012).
6. A. G. Kanani and S. H. Bahrami, *Trends Biomater. Artif. Organs.*, **24**, 93 (2010).
7. S. P. Zhong, Y. Z. Zhang, and C. T. Lim, *Wiley Interdiscip. Rev. Nanomed. Nanobiotechnol.*, **2**, 510 (2010).
8. P. Zahedi, I. Rezaeian, S.-O. Ranaei-Siadat, S.-H. Jafari, and P. Supaphol, *Polym. Adv. Technol.,* **21**, 77 (2010).
9. C.-M. Hsu and S. Shivkumar, *Macromol. Mater. Eng.,* **289**, 334 (2004).
10. Y.-F. Goh, I. Shakir, and R. Hussain, *J. Mater. Sci.,* **48**, 3027 (2013).
11. R. Morent, N. De Geyter, C. Leys, L. Gengembre, and E. Payen, *Text. Res. J.,* **77**, 471 (2007).
12. P. Amornsudthiwat, R. Mongkolnavin, S. Kanokpanont, J. Panpranot, C. San Wong, and S. Damrongsakkul, *Colloids Surfaces B Biointerfaces*, **111**, 579 (2013).
13. X. Lu, M. Laroussi, and V. Puech, *Plasma Sources Sci. Technol.,* **21**, 34005 (2012).
14. Q. Shi, N. Vitchuli, J. Nowak, Z. Lin, B. Guo, M. McCord, M. Bourham, and X. Zhang, *J. Polym. Sci. Part B Polym. Phys.,* **49**, 115 (2011).
15. M. Dadras Chomachayi, A. Solouk, S. Akbari, D. Sadeghi, F. Mirahmadi, and H. Mirzadeh, *J. Biomed. Mater. Res.-Part A*, **106**, 1092 (2018).
16. E. S. Gil, D. J. Frankowski, S. M. Hudson, and R. J. Spontak, *Mater. Sci. Eng. C*, **27**, 426 (2007).
17. P. Uttayarat, S. Jetawattana, P. Suwanmala, J. Eamsiri, T. Tangthong, and S. Pongpat, *Fiber. Polym.,* **13**, 999 (2012).
18. M. D. Chomachayi, A. Solouk, and H. Mirzadeh, *Prog. Biomater.,* **5**, 71 (2016).
19. S. Grande, J. Van Guyse, A. Y. Nikiforov, I. Onyshchenko, M. Asadian, R. Morent, R. Hoogenboom, and N. De Geyter, *ACS Appl. Mater. Interfaces*, **9**, 33080 (2017).
20. J. A. Davis, R. O. James, and J. O. Leckie, *J. Colloid Interface Sci.,* **63**, 480 (1978).
21. V. Colombo, D. Fabiani, M. L. Focarete, M. Gherardi, C. Gualandi, R. Laurita, and M. Zaccaria, *Plasma Process Polym.,* **11**, 247 (2014).
22. G. Jones and M. Dole, *J. Am. Chem. Soc.,* **51**, 2950 (1929).
23. W. E. Teo and S. Ramakrishna, *Nanotechnology*, **17**, 89 (2006).
24. T. Subbiah, G. S. Bhat, R. W. Tock, S. Parameswaran, and S. S. Ramkumar, *J. Appl. Polym. Sci.,* **96**, 557 (2005).
25. M. Di Foggia, P. Taddei, A. Torreggiani, M. Dettin, and A. Tinti, *Proteomics Res. J.,* **2**, 231 (2011).
26. X. Hu, D. Kaplan, and P. Cebe, *Macromolecules*, **39**, 6161 (2006).
27. Q. Lu, B. Zhang, M. Li, B. Zuo, D. L. Kaplan, Y. Huang, and H. Zhu, *Biomacromolecules*, **12**, 1080 (2011).
28. J. O. Warwicker, *Acta Crystallogr.,* **7**, 565 (1954).
29. R. E. Marsh, R. B. Corey, and L. Pauling, *Biochim. Biophys. Acta*, **16**, 1 (1955).
30. M. Gandhi, H. Yang, L. Shor, and F. Ko, *Polymer*, **50**, 1918 (2009).
31. A. Nova, S. Keten, N. M. Pugno, A. Redaelli, and M. J. Buehler, *Nano Lett.,* **10**, 2626 (2010).
32. S. A. Fossey, G. Némethy, K. D. Gibson, and H. A. Scheraga, *Biopolym. Orig. Res. Biomol.,* **31**, 1529 (1991).
33. M. F. Talbott, G. S. Springer, and L. A. Berglund, *J. Compos. Mater.,* **21**, 1056 (1987).
34. M. Wang, H.-J. Jin, D. L. Kaplan, and G. C. Rutledge, *Macromolecules*, **37**, 6856 (2004).
35. J. Zhou, C. Cao, and X. Ma, *Int. J. Biol. Macromol.,* **45**, 504 (2009).
36. A. L. Oliveira, L. Sun, H. J. Kim, X. Hu, W. Rice, J. Kluge, R. L. Reis, and D. L. Kaplan, *Acta Biomater.,* **8**, 1530 (2012).